ACCSCIENCE PUBLISHING
An International Journal of Optimization and Control: Theories & Applications
ISSN: 2146-0957 eISSN: 2146-5703
Vol.16, No.2, pp.517-530 (2026)
https://doi.org/10.36922/IJOCTA025460203
IJOCTA
RESEARCH ARTICLE

Bilinear neural network method for solving extended (2+1)-dimensional sixth-order benney-luke equation

Nguyen Minh Tuan* and Huynh Trong Thua*

Faculty of Information Technology, Posts and Telecommunications Institute of Technology, 11 Nguyen Dinh Chieu, Sai Gon ward, Ho Chi Minh City, Viet Nam
minhtuan@ptit.edu.vn, thuaht@ptit.edu.vn

ARTICLE INFO

Article History:
Received: November 12, 2025
Revised: December 4, 2025
Accepted: December 9, 2025
Published Online: January 12, 2026

Keywords:
Sixth-order Benney-Luke equation
bilinear neural network method
Hirota bilinear operator
(2+1)-dimensional Benney-Luke equation
Soliton solution
Analytic exact solution

AMS Classification 2010:
26A33; 34A08; 35H15; 34K50
47H10; 60H10

ABSTRACT

The Benney–Luke (BL) equation is a fundamental nonlinear evolution equation that models long-wave propagation in fluid dynamics and other nonlinear dispersive media. To understand more complex wave interactions and higher-order dispersive effects, extended forms of the BL equation have been developed, providing improved physical realism in describing nonlinear wave phenomena. Despite these advancements, existing studies on the extended sixth-order BL equation remain limited in the systematic construction of exact analytical solutions, particularly those encompassing diverse nonlinear structures such as rogue waves, lump waves, and peak-type solutions. This paper proposes a novel roadmap of the bilinear neural network method to derive new classes of exact solutions for the extended sixth-order Benney–Luke (BL) equation. Extended from previous models due to space-lower nonlinearities, the extended sixth-order equation incorporates additional dispersive and nonlinear interaction terms, enabling more comprehensive modeling of wave dynamics in fluid systems and nonlinear phenomena. Using Hirota's bilinear operator and a neural network-based framework, we construct a diverse spectrum of analytical solutions, including kink, rogue, lump, and peakon-type solitons. These solutions significantly expand the known solution space of the BL family and offer deeper physical insights into nonlinear wave behavior such as wave steepening, resonance, and dispersion. The extended equation not only bridges mathematical rigor and physical realism but also improves the computational efficiency and adaptability of neural network-based structures in analyzing nonlinear partial differential equations.

1. Introduction

Recently, a bilinear neural network construction for a fractional Konopelchenko–Dubrovsky-Kaup–Kupershmidt equation, a finite element scheme for a nanoscale heat transport analysis, a sine-Gordon expansion method for to nonlinear wave equation with beta-derivatives, and reliable methods for the (3 + 1)-dimensional chiral nonlinear Schrodinger equation have been proposed. Long water waves, especially those that are weakly nonlinear and weakly dispersive, give rise to a nonlinear partial differential equation NPDE known as the Benney–Luke equation. By more precisely simulating bidirectional wave propagation, it is an improvement over Boussinesq-type models. Many types of solutions have been obtained, such as precise traveling wave solutions to nonlinear evolution equations that play important roles in mathematical physics, science, and engineering. [1] The modified simple equation (MSE) technique, a reliable and useful mathematical tool, is an efficient way to

*Corresponding Author

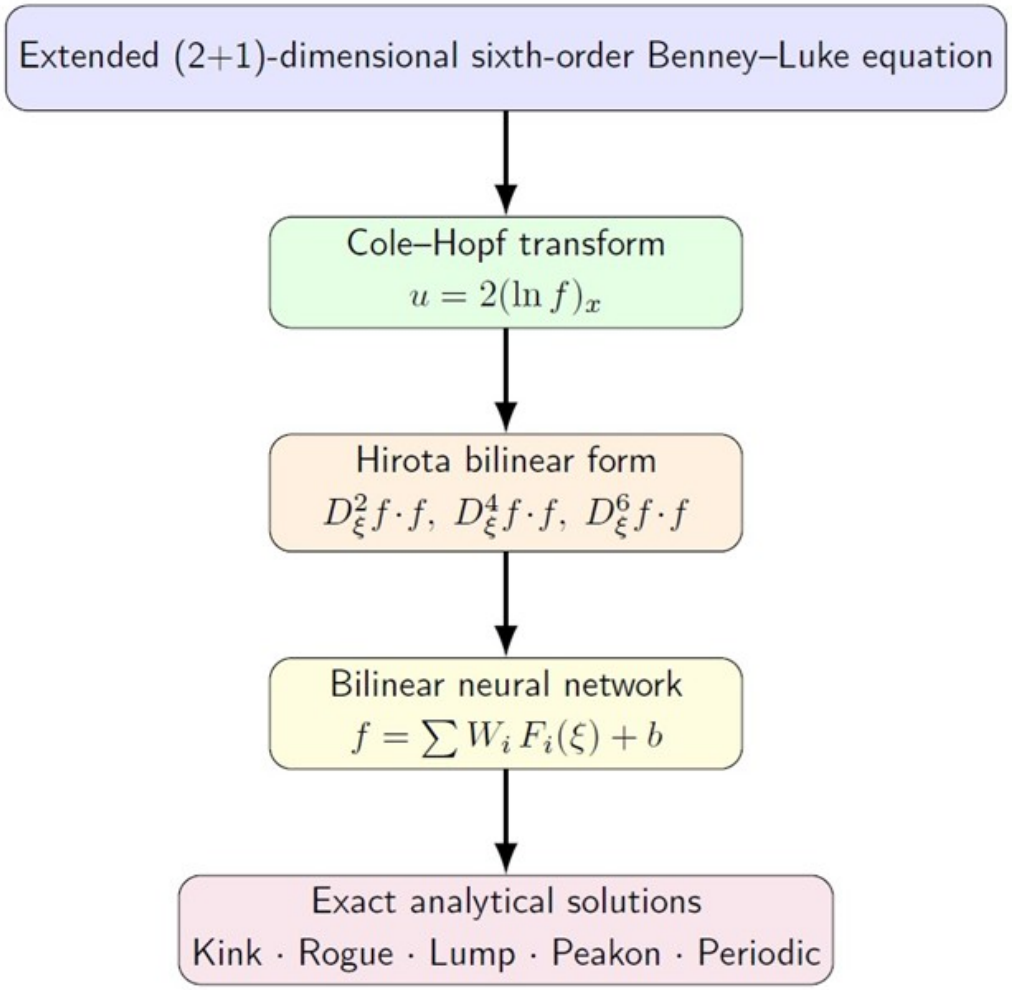

Figure 1. Graphical abstract using bilinear neural network method for solving extended (2+1)-dimensional sixth-order Benney–Luke equation

generate such solutions. The MSE method allows for precise solutions to nonlinear equations with parameters, such as the Benney–Luke and phi-4 equations. Exact traveling wave solutions can be used to generate solitary wave solutions when certain values are assigned.

Using the conformable fractional derivative framework, fractional derivatives have been added to the spatial and temporal variables to further extend the Benney–Luke equation. A range of solution structures, including exponential, trigonometric, and hyperbolic functions, have been generated by combining fractional calculus with the MSE method.[3] Furthermore, accurate solutions of the Benney–Luke equation in hyperbolic form have been obtained using the (1/G')-expansion method.[4] Additionally, the Tanh Ansatz approach has been applied, which uses a straightforward compatible wave transformation in one dimension to reduce the governing equations to integer-order ordinary differential equations. The Ansatz method is then used to generate precise analytical solutions, with examples showing the impact of selected parameter values and derivative orders.[5] The novel generalised rational function method can be used to find new solitary wave solutions for the Benney–Luke problem and the Phi-4 equation. The stability of the governing equations is further examined using the linear stability analysis feature.[6] We used the tanh–coth method to obtain specific traveling wave solutions for two well-known nonlinear Sobolev-type partial differential equations: the higher-order improved Boussinesq equation and the Benney–Luke equation.[7]

The sn-ns technique was used to generate novel solutions for this problem. Next, we offer solutions for elliptic and trigonometric functions as well as hyperbolic functions that can be found using the Tanh–Coth approach. This method allows for the simultaneous derivation of three different types of solutions.[8] The improved (G'/G)-expansion approach can be used to solve the NPDE of the Benny-Luke equation, resulting in new and more comprehensive closed-form wave

solutions. This is one of the powerful methods that have recently been developed to create more accurate wave solutions for NPDEs. We have obtained a number of novel exact solutions expressed in terms of trigonometric and hyperbolic functions. Among these are solutions for soliton and arbitrary parameterized periodic waves.[9,10]

The Benney–Luke equation is given as follows:[8,11]

$$u_{tt} - u_{xx} + au_{xxxx} - bu_{xxtt} + nu_t(u_x)^{n-1}u_{xx} + 2\left(u_x\right)^n u_{tx} = 0, \quad (1)$$

where $a - b = \sigma - \frac{1}{3}$; $n \in \mathbb{N}$; a, b are the specified positive values that satisfy the requirement; and σ represents the Bond number that regulates the relationship between the gravitational force and an object's surface tension.

In another study, new solitary wave solutions of their fractional order versions of two nonlinear evolution equations from mathematical physics and engineering—the Benny-Luke equation and the Phi-4 equation—were extracted using the (G'/G)-expansion method in combination with a modified Riemann–Liouville fractional operator. Rational, hyperbolic, and trigonometric function solutions are among the exact solutions.[12] Additionally, different solutions of the Benney–Luke equation are obtained in terms of hyperbolic functions, traveling wave solutions,[13] and soliton solutions[11] utilizing the (G'/G,1/G)-technique, Lagrangian formulation, and bilinear neural network method. A machine learning approach is used by the BNNM[14] to construct solutions based on the Hirota bilinear operator.[15,16]

Neural network techniques, such as the multivariate BNNM[17] and the physics-informed neural network method,[18,19] make up the particular structure of machine learning. The BNNM is simple, flexible, and capable of handling many approaches and solutions.[20,21] Simplifying the equation is a reasonable way to reduce computational performance. The Benney–Luke equation, which has been studied in a (1+1)-dimensional model in earlier research, has a limited solution for various forms of water wave propagation. This study aims to solve the sixth-order Benney–Luke problem generated in a (2+1)-dimensional space, offering a greater variety of solutions.

To obtain the exact analytical solutions, this work creates a new extended (2+1)-dimensional sixth-order Benney–Luke equation[22] as follows:

$$u_{tt} - u_{xx} + au_{xxxx} - bu_{xxtt} + 2u_tu_xu_{xx} + 2\left(u_x\right)^2 u_{tx} + ru_x.u_{xx} + p\left(u_{xx}u_{xxx} + u_x.u_{xxxx}\right) + qu_{xxxxxx} + su_{yy} = 0. \quad (2)$$

A popular application of the performance of the Hirota bilinear form is to find n-soliton solutions of the integrable nonlinear equations, which helps reduce the laborious expression of NPDEs [23]. Utilizing the Hirota bilinear expression, which is given by:[15]

$$D_x\left(f \cdot g\right) = \left(\frac{\partial}{\partial x} - \frac{\partial}{\partial x'}\right) f\left(x\right) \cdot g\left(x'\right)\Big|_{x=x'}, \quad (3)$$

or, in general,

$$D_x^m D_t^n\left(f \cdot g\right) = \left(\frac{\partial}{\partial x} - \frac{\partial}{\partial x'}\right)^m \left(\frac{\partial}{\partial t} - \frac{\partial}{\partial t'}\right)^n f\left(x\right) \cdot g\left(x'\right)\Big|_{x=x',t=t'},$$

where the Hirota derivative operator, denoted by D, is a binary operator.

The Hirota bilinear form's compact operator can be written as:

$$D_x^m\left(f \cdot g\right) = \sum_{r=0}^{m} (-1)^r \begin{pmatrix} m \\ r \end{pmatrix} f_{(r-m)x} \cdot g_{rx}, \quad (4)$$

where the binomial coefficient is

$$\begin{pmatrix} m \\ r \end{pmatrix} = \frac{m!}{r!\left(m-r\right)!}, 0 \leq r \leq m. \quad (5)$$

The classical Benney–Luke equation is an established bidirectional model for weakly nonlinear and weakly dispersive waves, providing less computation and solutions. However, the standard fourth-order formulation cannot fully describe many physical scenarios where higher-order dispersion, multidimensional effects, and strong nonlinear interactions are significant. Motivated by these limitations, this work develops an extended sixth-order (2+1)-dimensional Benney–Luke equation that incorporates additional dispersive and nonlinear terms. These extensions naturally arise from higher-order asymptotic expansions of the Euler equations and allow the model to capture richer wave behaviors such as rogue-wave focusing, multi-scale dispersion, and peakon formation. Furthermore, classical analytic methods are often limited to specific trial functions. The BNNM provides a flexible and systematic framework that combines Hirota's bilinear form with neural-network-style functional construction. This motivates the present study: to unify physical realism, high-order mathematical modeling, and neural-network-inspired exact-solution generation to produce new classes of analytical solutions that were previously inaccessible.

2. Methodology

The method proposed in this study is constructed as shown in Figure 1. Figure 2 illustrates the general process of the neural network

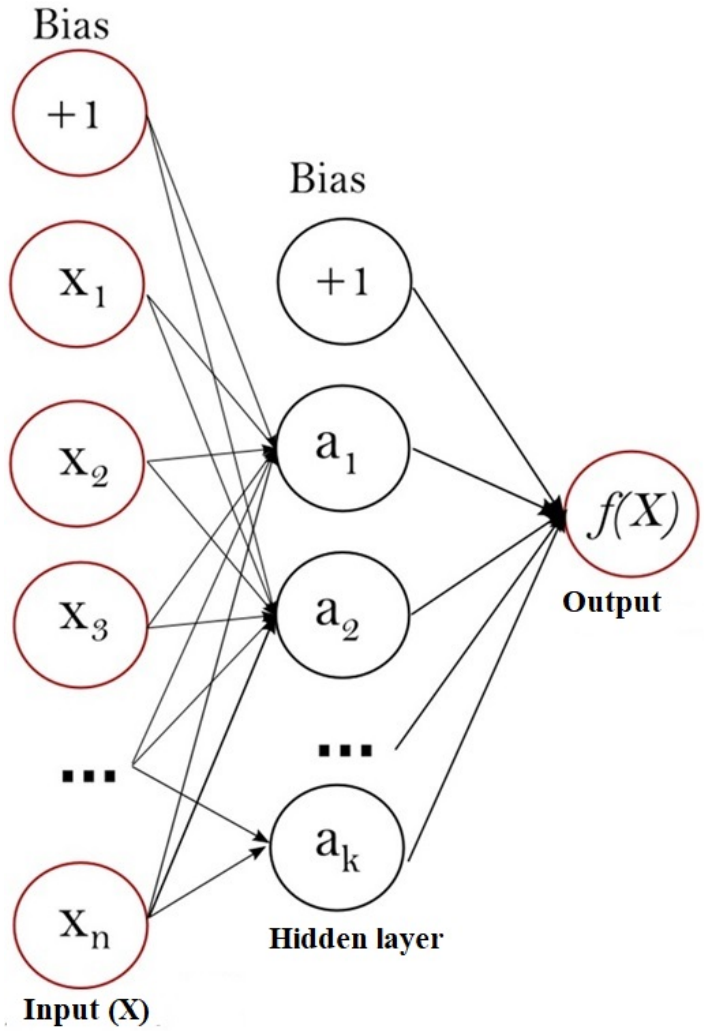

Figure 2. Neural network model at the state k

model, which consists of the input layer $X_i, i = 1, \cdots, n$; the hidden layer H_{k-1}, H_k, H_{k+1}; including $a_1, a_2, \cdots, a_k$; and the active functions that copy data from the previous state $k-1$ and concatenate at present state t to produce the output at state $k+1$. Recurrent and intrinsic activation is the hidden layer's primary method of reconstructing the input data, which is expressed as follows:

$$H_k = f\left(X_{k-1}W_{xk} + H_kW_{hh} + b_h\right) \tag{6}$$

The neural network model's function can be represented as a sequence indexed by the input layer state k, which is then concatenated with the function x_k. The first hidden layer, h_{k-1}, was calculated after the weights w_{xh}, w_{hh} were determined, and the second hidden layer, h_k, b_q, represents the processing bias. The resulting output is displayed as follows:

$$x_k = h_{k-1}w_{xh} + h_kw_{hh} + b_q \tag{7}$$

The BNNM was built as follows:

Step 1: NPDEs can be transformed into the equation of Hirota bilinear form using the Cole–Hopf transform $u = 2(lnF)_x$ by utilizing Equations (3)–(5). This step incorporates the traveling transform into the necessary bilinear terms as follows:

$$F(f, f_t, f_x, f_y, f_{xx}, f_{xt}, f_{yt}, \cdots) = 0 \tag{8}$$

where $f_t, f_x, f_y, f_{xx}, f_{xt}, f_{yt}, \cdots$ denote the derivative in terms of $t, x, y, xx, xt, yt, \cdots$, respectively.

Step 2 : Create the output function f sequence in the form of Equation (6) & Equation (7) using the appropriate functions for weights and active functions, as illustrated in Figure 2. Replace Equation (8) with the output function, compile the weight coefficients, and apply bias to get algebraic equation systems.

Step 3 : The Hirota bilinear equation can be satisfied by classifying the test functions and solving the simultaneous equations in terms of weights and bias.

Step 4 : The output function acquired in terms of weight and active functions is incorporated into the NPDE systems.

Step 5 : Change the function in the Cole–Hopf transform to produce accurate solutions that satisfy the Birota bilinear equation as well as the NPDEs.

3. The Hirota bilinear transform of the Benney–Luke equation

From Equation (2), taking the traveling transformation $\xi = x + kt + hy$, we have:

$$\begin{aligned}&\left(k^2-1\right)u'' + \left(a-bk^2\right)u'''' + 2k\left(u'\right)^2 u''\\&+ 2k\left(u'\right)^2 u'' + ru'.u'' + p\left(u''u''' + u'.u''''\right)\\&+ qu''''''' + sh^2u'' = 0.\end{aligned} \tag{9}$$

Using the transformation $u = 2w_\xi, w = \ln f$, and we have

$$\begin{aligned}&2\left(k^2-1\right)w_{\xi\xi\xi} + 2\left(a-bk^2\right)w_{\xi\xi\xi\xi\xi} + 32k\left(w_{\xi\xi}\right)^2 w_{\xi\xi\xi}\\&+ 4rw_{\xi\xi}.u_{\xi\xi\xi} + 4p\left(w_{\xi\xi\xi}w_{\xi\xi\xi\xi\xi} + w_{\xi\xi}.w_{\xi\xi\xi\xi\xi}\right)\\&+ 2qw_{\xi\xi\xi\xi\xi\xi\xi} + sh^2u_{\xi\xi} = 0.\end{aligned} \tag{10}$$

Integrating both sides of the equation, we have:

$$\begin{aligned}&\left(k^2-1\right)w_{\xi\xi} + \left(a-bk^2\right)w_{\xi\xi\xi\xi} + \frac{16k}{3}\left(w_{\xi\xi}\right)^3\\&+ ru_{\xi\xi}^2 + 2pu_{\xi\xi}.u_{\xi\xi\xi\xi}\\&+ qu_{\xi\xi\xi\xi\xi\xi} + sh^2u_{\xi\xi} = 0.\end{aligned} \tag{11}$$

Using definitions from Equation 3 to Equation 5, Equation (11) can be rewritten as:

$$\begin{aligned}-\left(1-k^2\right)D_\xi^2 + b\left(1-k^2\right)D_\xi^4 + qD_\xi^6\\+ sh^2D_\xi^2 = 0.\end{aligned} \tag{12}$$

Equation (12) is simplified as follows:

$$-(1-n)D_\xi^2 + bD_\xi^4 + mD_\xi^6 = 0, \tag{13}$$

where

$$\begin{aligned}&D_\xi^4 f\cdot f = 2(ff_{\xi\xi\xi\xi} - 4f_\xi f_{\xi\xi\xi} + 3f_{\xi\xi}^2),\\&D_\xi^6 f\cdot f =\\&2(ff_{\xi\xi\xi\xi\xi\xi} - 6f_\xi f_{\xi\xi\xi\xi\xi} + 15f_{\xi\xi}f_{\xi\xi\xi\xi} - 10f_{\xi\xi\xi}^2),\\&D_\xi^2 f\cdot f = 2(ff_{\xi\xi} - (f_\xi)^2),\end{aligned}$$

and

$$3p = 4k; 45q = 4k; r = 6b(1-k^2); m = \frac{q}{1-k^2};$$
$$n = \frac{sh^2}{1-k^2}.$$

4. Solutions form of the extended Benney–Luke equation

Using the model depicted in Figure 2, we constructed the output function F as the sum of the product of weights $W_{h,f}$ and test functions $F_h\left(\xi_h\right)$, including the bias b_h, as follows:

$$F = W_{h,f}F_h\left(\xi_h\right) + b_h, \tag{14}$$

where $F_h\left(\xi_h\right)$ is considered as the function of hidden states. To facilitate the procedure, we extracted layer slices by aggregating the weights $w_{h_ij}, i = 1,\cdots,n; j = 1,\cdots,m$, the active function $f_{h_{i-1}}\left(\xi_{h_{i-1}}\right)$, and the bias b_j as follows:

$$\begin{aligned}&\xi_{h_i} = w_{h_ij}f_{h_{i-1}}\left(\xi_{h_{i-1}}\right) + b_j, i = 1,\cdots,n;\\&j = 1,\cdots,m.\end{aligned} \tag{15}$$

where $h_i, i = 1,\cdots,n$ is the state of the process. In this section, the neural network is constructed using the trial functions listed in Table 1. These trial functions are substituted into Equation (13) to determine the weights and solve for the activation functions, as shown in Equations(14) and (15).

4.1. Model 3-1-1

This model includes three neurons of the input layers, one neuron of the hidden layer, and one neuron of the output layers.
Given the trial function in Case IV (Table 1), the one-soliton solutions are shown as follows:

$$u_{11} = \frac{2a_{11}b_{11}e^{b_{11}(x+kt+hy)+b_{12}}}{a_{01} + a_{11}e^{b_{11}(x+kt+hy)+b_{12}}}$$

and

$$u_{12} = -\frac{2a_{11}b_{11}e^{-b_{11}(x+kt+hy)-b_{12}}}{a_{01} + a_{11}e^{-b_{11}(x+kt+hy)-b_{12}}}.$$

where $b = \frac{4kb_{11}^4+45sh^2+45k^2-45}{45b_{11}^2(k^2-1)}$.

The graph of u_{11} is depicted in Figures 3 and 4.

4.2. Model 3-2-1

This model includes three neurons in the input layers, two neurons of the hidden layer, and 1 neuron in output layer.
Given the trial function in Case IV (Table 1). The one-soliton solutions are obtained as follows:

$$u_{21} = \frac{2a_{21}\left(b_{21}+c_{21}\right)e^{b_{21}(x+kt+hy)+c_{21}(x+kt+hy)+c_{22}+b_{22}}}{a_0 + a_{11}e^{b_{11}(x+kt+hy)+c_{11}(x+kt)+c_{22}+b_{22}}},$$

and

$$u_{22} = \frac{2a_{21}\left(-b_{21}-c_{21}\right)e^{-b_{21}(x+kt+hy)-c_{21}(x+kt+hy)-c_{22}-b_{22}}}{a_0 + a_{11}e^{-b_{21}(x+kt+hy)-c_{21}(x+kt+hy)-c_{22}-b_{22}}},$$

where
$b = \frac{4kb_{21}^4+16b_{21}^3c_{21}k+24b_{21}^2c_{21}^2k+16b_{21}c_{21}^3k+4c_{11}^4k+45sh^2+45k^2-45}{45b_{21}^2k^2+90b_{21}c_{21}k^2+45c_{11}^2k^2-45b_{21}^2-90b_{21}c_{21}-45c_{21}^2}$.
The graph of u_{21} is depicted in Figures 5 and 6.

4.3. Model 3-1-1

This model includes three neurons of input layer, one neuron of the hidden layer, and one neuron of the output layer.

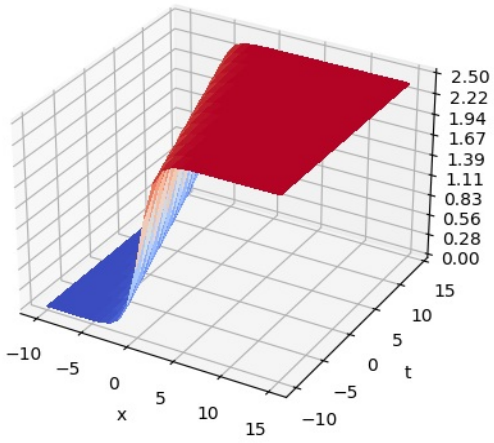

Figure 3. Kink solution u_{11} when $a_{01} = 0.2; b_{11} = 1.2; a_{11} = 1.3; b_{12} = 1.1; k = 0.2; h = 0.3; s = 0.1; t = 0.5$

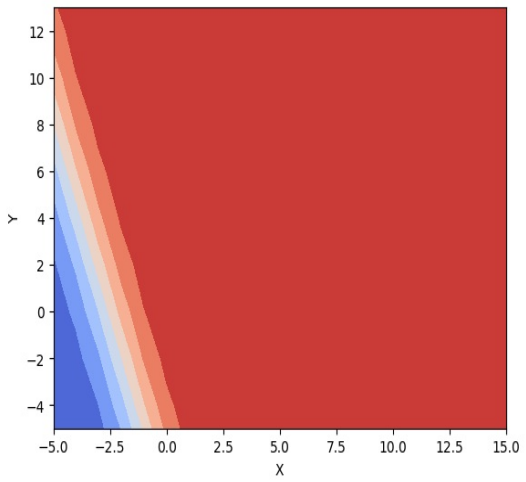

Figure 4. Contour graph of solution u_{11} when $a_{01} = 0.2; b_{11} = 1.2; a_{11} = 1.3; b_{12} = 1.1; k = 0.2; h = 0.3; s = 0.1; t = 0.5$

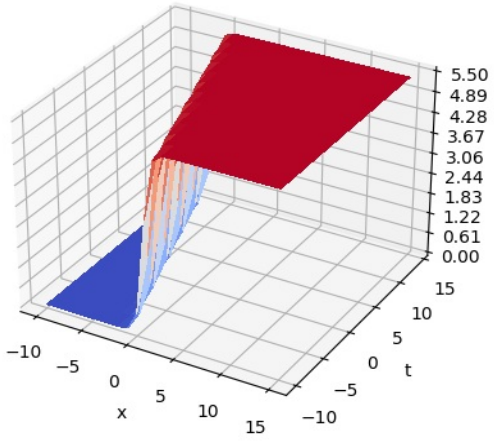

Figure 5. Kink solution u_{21} when $a_{02} = 0.2; b_{21} = 1.2; a_{21} = 1.3; b_{22} = 1.1; c_{21} = 1.5; k = 0.2; h = 0.3; s = 0.1; t = 0.5$

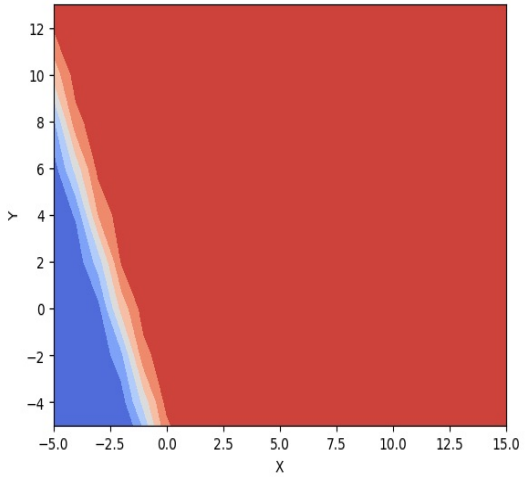

Figure 6. Contour graph of solution u_{21} when $a_{02} = 0.2; b_{21} = 1.2; a_{21} = 1.3; b_{22} = 1.1; c_{21} = 1.5; k = 0.2; h = 0.3; s = 0.1; t = 0.5$

Given the trial function in Case II (Table 1). The hyperbolic solutions are attained as follows:

$$u_{31} = \frac{2a_{31}b_{31}\cosh\left(b_{31}\left(x+kt+hy\right)+b_{32}\right)}{a_0 + a_{31}\sinh\left(b_{31}\left(x+kt\right)+b_{32}\right)},$$

and

$$u_{31} = \frac{2a_{31}b_{31}\sinh\left(b_{31}\left(x+kt+hy\right)+b_{32}\right)}{a_0 + a_{31}\cosh\left(b_{31}\left(x+kt+hy\right)+b_{32}\right)},$$

where $b = \frac{4b_{31}^2 k}{9(k^2-1)}$ and $s = \frac{16b_{31}^4 k - 45k^2 + 45}{45h^2}$. The graph of u_{31} is depicted in Figures 7 and 8.

4.4. Model 3-1-1

This model includes three neurons of the input layer, one neuron of the hidden layer, and one neuron of the output layer.
Given the trial function as Case III (Table 1), the trigonometry solution is obtained as follows:

$$u_{41} = \frac{2a_{41}b_{41}\cos\left(b_{41}\left(x+kt+hy\right)+b_{42}\right)}{a_{04} + a_{41}\sin\left(b_{41}\left(x+kt+hy\right)+b_{42}\right)}$$

and

$$u_{41} = \frac{2a_{41}b_{41}\sin\left(b_{41}\left(x+kt+hy\right)+b_{42}\right)}{a_{04} + a_{41}\cos\left(b_{41}\left(x+kt+hy\right)+b_{42}\right)},$$

where $b = -\frac{4b_{41}^2 k}{9(k^2-1)}$, and $s = \frac{16b_{41}^4 k - 45k^2 + 45}{45h^2}$. The graph of u_{41} is shown in Figures 9 and 10.

4.5. Model 3-2-4

This model includes three neurons of the input layer, two neurons of the hidden layer, and four neurons of the output layer.
Given the trial function in Case VII (Table 1) the 2-soliton solution u_{51} is presented in Table 2,

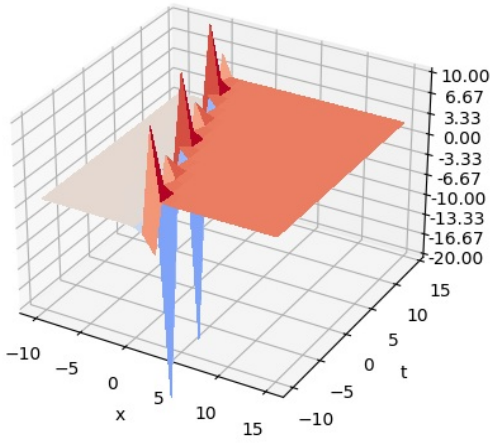

Figure 7. Rogue solution u_{31} when $a_{03} = 0.2; b_{31} = 1.2; a_{31} = 1.3; b_{32} = 1.1; c_{31} = 1.5; k = 0.2; h = 0.3; s = 0.1; t = 0.5$

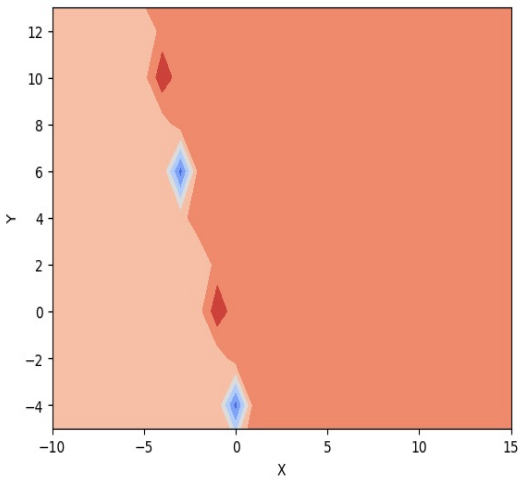

Figure 8. Contour graph of solution u_{31} when $a_{03} = 0.2; b_{31} = 1.2; a_{31} = 1.3; b_{32} = 1.1; c_{31} = 1.5; k = 0.2; h = 0.3; s = 0.1; t = 0.5$

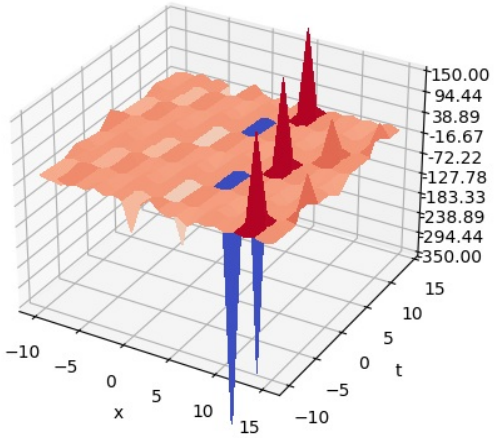

Figure 9. Rogue solution u_{41} when $k = 0.5; a_{04} = 0.2; a_{41} = 1.3; b_{41} = 1.5; b_{42} = 1.1; h = 0.3; s = 0.1; t = 0.5$

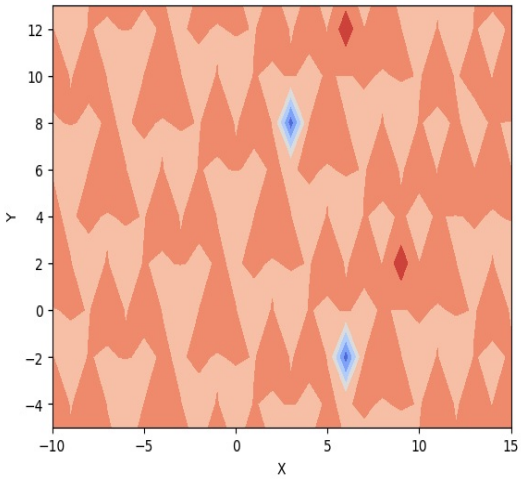

Figure 10. Contour graph of solution u_{41} when $k = 0.5; a_{04} = 0.2; a_{41} = 1.3; b_{41} = 1.5; b_{42} = 1.1; h = 0.3; s = 0.1; t = 0.5$

where $b = \frac{16c_{51}^2 k}{9(k^2-1)}, s = \frac{256c_{51}^4 k - 45k^2 + 45}{45h^2}$. The graph of u_{51} is depicted in Figures 11 and 12.

4.6. Model 3-2-3

This model includes three neurons of the input layer, two neurons of the hidden layer, and three neurons of the output layer.
Given the trial function in Case VIII (Table 1), the trigonometry 2-soliton solution attained as follows, where $b = \frac{8\left(b_{61}^2 - c_{61}^2\right)k}{45(k^2-1)}, s = \frac{4b_{61}^2 k + 8b_{61}^2 c_{61}^2 k + 4c_{61}^4 k - 45k^2 + 45}{45h^2}$,

$a_{11} = \frac{a_{62}^2 c_{61}^2 \left(b_{61}^2 + 9c_{61}^2\right)}{4a_{63} b_{61}^2 \left(9b_{61}^2 + c_{61}^2\right)}$.
The graph of u_{61} is depicted in Figures 13 and 14.

4.7. Model 3-2-3

This model includes three neurons of input layers, two neurons of hidden layer, and three neurons of the output layers.
Given the trial function in Case V (Table 1), the test function is attained as follows: $f = a_{07} + a_{71}e^{\xi_1} + a_{72}e^{\xi_2} + a_{73}e^{\xi_1+\xi_2}; \xi_1 = b_{71}xi + b_{72}; \xi_2 = c_{71}xi + c_{72}$, where $a_{71} = \frac{a_{73}(2b_{71}+c_{71})(b_{71}+c_{71})^2 a_{07}(b_{71}+2c_{71})}{(b_{71}-c_{71})^2 a_{72}(2b_{71}-c_{71})(b_{71}-2c_{71})}; b =$

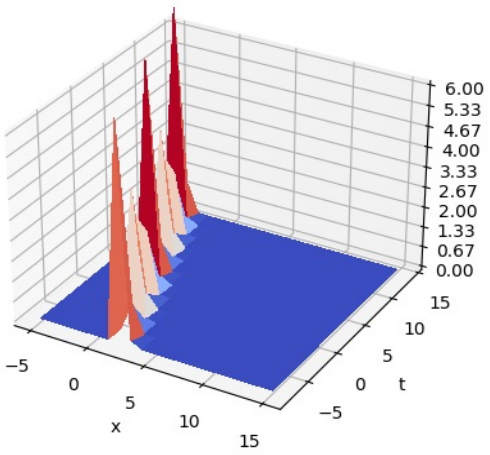

Figure 11. Lump solution u_{51} when $k = 0.5; a_{05} = 0.2; a_{51} = 1.3; a_{52} = 1.4; b_{51} = 3.7; b_{52} = 0.9; c_{51} = 0.6; c_{52} = 0.1$

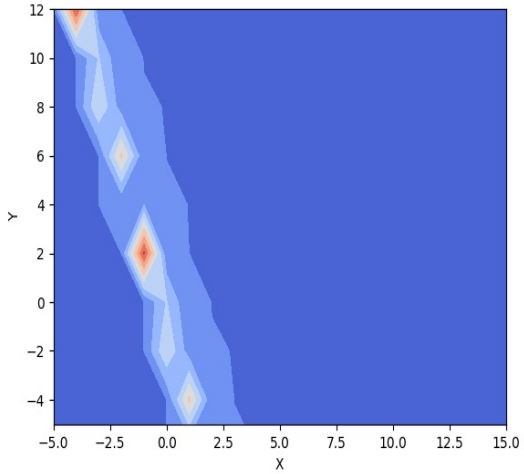

Figure 12. Contour graph of solution u_{51} when $k = 0.5; a_{05} = 0.2; a_{51} = 1.3; a_{52} = 1.4; b_{51} = 3.7; b_{52} = 0.9; c_{51} = 0.6; c_{52} = 0.1$

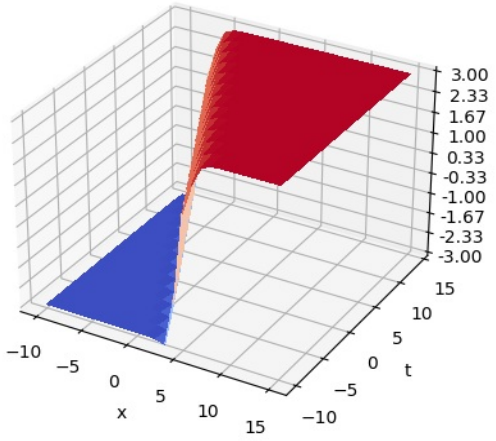

Figure 13. Kink solution u_{61} when $k = 0.5; a_{06} = 0.2; a_{61} = 1.3; a_{62} = 1.4; b_{61} = 3.7; b_{62} = 0.9; c_{61} = 0.6; c_{62} = 0.1$

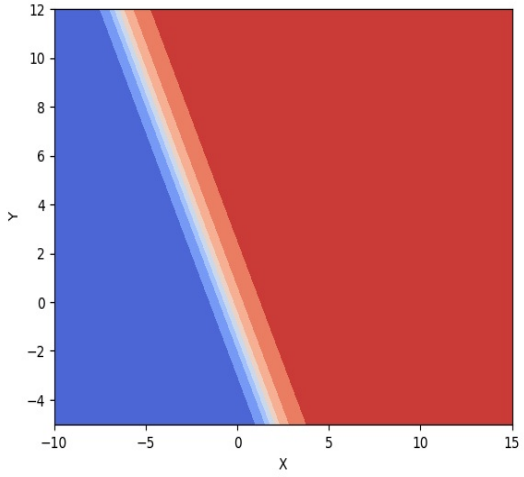

Figure 14. Contour graph of solution u_{61} when $k = 0.5; a_{06} = 0.2; a_{61} = 1.3; a_{62} = 1.4; b_{61} = 3.7; b_{62} = 0.9; c_{61} = 0.6; c_{62} = 0.1$

$\frac{4b_{71}^4k+45h^2s+45k^2-45}{45(k^2-1)b_{71}^2};$

$s = \big(72a_{07}^2a_{73}^2b_{71}^8k + 300a_{07}^2a_{73}^2b_{71}^7c_{71}k$

$+ 468a_{07}^2a_{73}^2b_{71}^6c_{71}^2k + 360a_{07}^2a_{73}^2b_{71}^5c_{71}^3k+$

$60a_{07}^2a_{73}^2b_{71}^4c_{71}^4k - 84a_{07}^2a_{73}^2b_{71}^3c_{71}^5k-$

$24a_{07}^2a_{73}^2b_{71}^2c_{71}^6k - 24a_{07}a_{71}a_{72}a_{73}b_{71}^8k+$

$548a_{07}a_{71}a_{72}a_{73}b_{71}^7c_{71}k - 372a_{07}a_{71}a_{72}a_{73}b_{71}^6c_{71}^2k+$

$960a_{07}a_{71}a_{72}a_{73}b_{71}^5c_{71}^3k - 324a_{07}a_{71}a_{72}a_{73}b_{71}^4c_{71}^4k+$

$28a_{07}a_{71}a_{72}a_{73}b_{71}^3c_{71}^5k-$

$48a_{07}a_{71}a_{72}a_{73}b_{71}^2c_{71}^6k - 48a_{71}^2a_{72}^2b_{71}^8k+$

$232a_{71}^2a_{72}^2b_{71}^7c_{71}k - 456a_{71}^2a_{72}^2b_{71}^6c_{71}^2k+$

$480a_{71}^2a_{72}^2b_{71}^5c_{71}^3k - 252a_{71}^2a_{72}^2b_{71}^4c_{71}^4k+$

$56a_{71}^2a_{72}^2b_{71}^3c_{71}^5k - 12a_{71}^2a_{72}^2b_{71}^2c_{71}^6k-$

$810a_{07}^2a_{73}^2b_{71}^4k^2 - 2295a_{07}^2a_{73}^2b_{71}^3c_{71}k^2-$

$1080a_{07}^2a_{73}^2b_{71}^2c_{71}^2k^2 + 675a_{07}^2a_{73}^2b_{71}c_{71}^3k^2+$

$270a_{07}^2a_{73}^2c_{71}^4k^2 + 270a_{07}a_{71}a_{72}a_{73}b_{71}^4k^2-$

$4095a_{07}a_{71}a_{72}a_{73}b_{71}^3c_{71}k^2 + 1350a_{07}a_{71}a_{72}a_{73}b_{71}^2c_{71}^2k^2-$

$225a_{07}a_{71}a_{72}a_{73}b_{71}c_{71}^3k^2 + 540a_{07}a_{71}a_{72}a_{73}c_{71}^4k^2$

$+ 540a_{71}^2 \times a_{72}^2b_{71}^4k^2 - 1710a_{71}^2a_{72}^2b_{71}^3c_{71}k^2$

$+ 1485a_{71}^2a_{72}^2b_{71}^2c_{71}^2k^2 - 450a_{71}^2a_{72}^2b_{71}c_{71}^3k^2+$

$135a_{71}^2a_{72}^2c_{71}^4k^2 + 810a_{07}^2a_{73}^2b_{71}^4+$

$2295a_{07}^2a_{73}^2b_{71}^3c_{71} + 1080a_{07}^2a_{73}^2b_{71}^2c_{71}^2-$

$675a_{07}^2a_{73}^2b_{71}c_{71}^3 - 270a_{07}^2a_{73}^2c_{71}^4-$

$270a_{07}a_{71}a_{72}a_{73}b_{71}^4 + 4095a_{07}a_{71}a_{72}a_{73}b_{71}^3c_{71}-$

$1350a_{07} \times a_{71}a_{72}a_{73}b_{71}^2c_{71}^2+$

$225a_{07}a_{71}a_{72}a_{73}b_{71}c_{71}^3 - 540a_{07}a_{71}a_{72}a_{73}c_{71}^4$

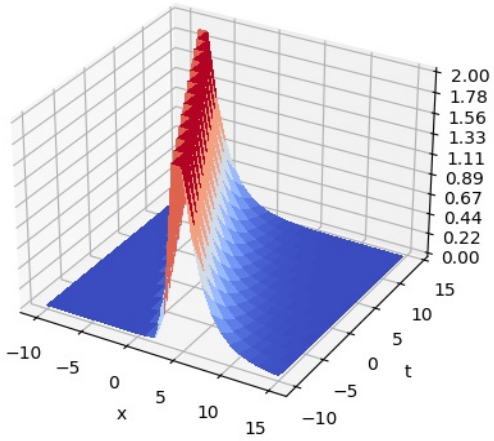

Figure 15. Peakon solution u_{71} when $k = 0.5; a_{07} = 0.2; a_{71} = 1.3; b_{71} = 1.5; b_{72} = 1.1; c_{71} = 0.3; c_{72} = 1.7; a_{73} = 1.2; a_{72} = 1.7; h = 1.2; t = 1.3$

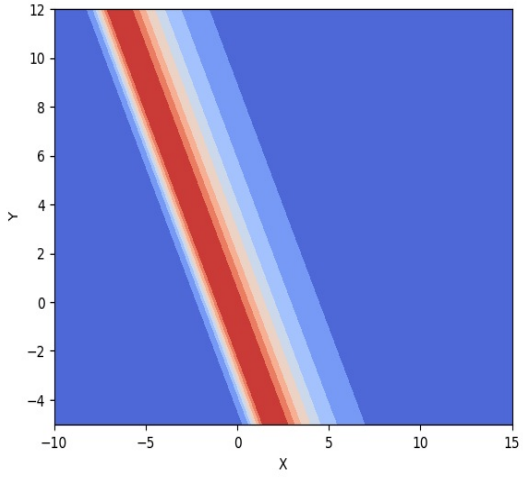

Figure 16. Contour graph of solution u_{71} when $k = 0.5; a_{07} = 0.2; a_{71} = 1.3; b_{71} = 1.5; b_{72} = 1.1; c_{71} = 0.3; c_{72} = 1.7; a_{73} = 1.2; a_{72} = 1.7; h = 1.2; t = 1.3$

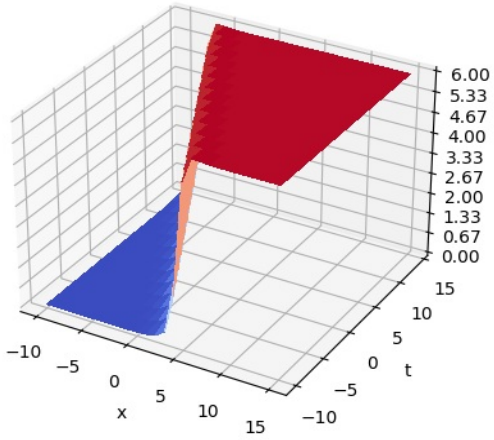

Figure 17. Kink solution u_{81} when $k = 0.5; a_{08} = 0.2; a_{81} = 1.3; a_{82} = 1.4; b_{81} = 3.7; b_{82} = 0.9; c_{81} = 0.6; c_{82} = 0.1$

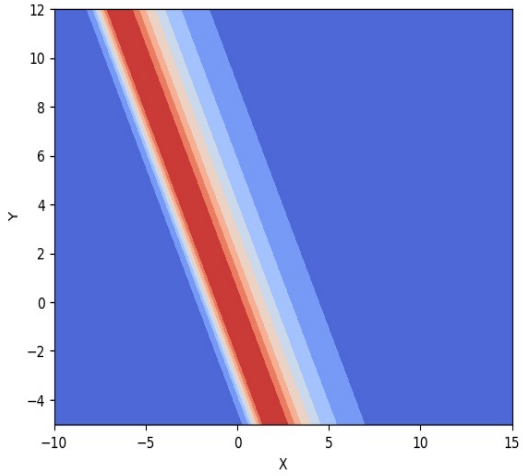

Figure 18. Contour graph of solution u_{81} when $k = 0.5; a_{08} = 0.2; a_{81} = 1.3; a_{82} = 1.4; b_{81} = 3.7; b_{82} = 0.9; c_{81} = 0.6; c_{82} = 0.1$

$$
\begin{aligned}
&-540a_{71}^2a_{72}^2b_{71}^4+1710a_{71}^2a_{72}^2b_{71}^3c_{71}-\\
&1485a_{71}^2a_{72}^2b_{71}^2c_{71}^2+450a_{71}^2a_{72}^2b_{71}c_{71}^3-\\
&135a_{71}^2a_{72}^2c_{71}^4)/(45h^2(18a_{07}^2a_{73}^2b_{71}^4+\\
&51a_{07}^2a_{73}^2b_{71}^3c_{71}+24a_{07}^2a_{73}^2b_{71}^2c_{71}^2-\\
&15a_{07}^2a_{73}^2b_{71}c_{71}^3-6a_{07}^2a_{73}^2c_{71}^4-\\
&6a_{07}a_{71}a_{72}a_{73}b_{71}^4+91a_{07}a_{71}a_{72}a_{73}b_{71}^3c_{71}-\\
&30a_{07}a_{71}a_{72}a_{73}b_{71}^2c_{71}^2+\\
&5a_{07}a_{71}a_{72}a_{73}b_{71}c_{71}^3-12a_{07}a_{71}a_{72}a_{73}c_{71}^4-\\
&12a_{71}^2a_{72}^2b_{71}^4+38a_{71}^2a_{72}^2b_{71}^3c_{71}-\\
&33a_{71}^2a_{72}^2b_{71}^2c_{71}^2+10a_{71}^2a_{72}^2b_{71}c_{71}^3-\\
&3a_{71}^2a_{72}^2c_{71}^4)).
\end{aligned}
$$

The graph of u_{71} is depicted in Figures 15 and 16.

4.8. Model 3-2-3

This model includes three neurons of the input layers, two neurons of the hidden layer, and three neurons of the output layers.
Given the trial function in Case IX (Table 1), the trial function is given by $f_{81} = a_{81}e^{\xi_1}(\sin(\xi_2) + a_{83}\cosh(\xi_1))$. We obtain the solutions as follows:

where $b = \frac{8k(b_{81}^2-c_{81}^2)}{45(k^2-1)}; s = \frac{4b_{81}^4k+8b_{81}^2c_{81}^2k+4c_{81}^4k-45k^2+45}{45h^2}$;
$a_{83} = \pm\frac{\sqrt{(9b_{81}^2+c_{81}^2)(b_{81}^2+9c_{81}^2)}c_{81}}{(9b_{81}^2+c_{81}^2)b_{81}}$.

The graph of u_{81} is depicted in Figures 17 and 18.

The physical performance of the solutions is as follows:

Table 1. Trial functions used in the bilinear neural network method

Cases	Names of the functions	Trial functions
I	$\tanh-\coth$ solutions[23]	$f_{11}=a_{01}+a_{11}\tanh(\alpha\xi)$ $f_{12}=a_{01}+a_{11}\coth(\alpha\xi)$
II	$\sinh-\cosh$ solutions[23]	$f_{11}=a_{01}+a_{11}\sinh(\alpha\xi)$ $f_{12}=a_{01}+a_{11}\cosh(\alpha\xi)$
III	$\sin-\cos$ solutions[23]	$f_{11}=a_{01}+a_{11}\sin^{\beta}(\mu\xi)$ $f_{12}=a_{01}+a_{11}\cos^{\beta}(\mu\xi)$
IV	1-soliton solution[23]	$f_{11}=a_{01}+a_{11}e^{\alpha\xi}$
V	3-soliton solution[23]	$f_{11}=a_{01}+a_{11}e^{\alpha\xi_1}+a_{12}e^{h\xi_2}+a_{13}e^{p\xi_3}+a_{14}e^{q(\xi_1+\xi_2)}$ $+a_{15}e^{r(\xi_2+\xi_3)}+a_{16}e^{l(\xi_1+\xi_3)}+a_{17}e^{m(\xi_1+\xi_2+\xi_3)}$
VI	n-soliton solution[23]	$f_{11}=a_{01}+\sum_{i=1}^{N}a_i\exp(k_i\xi_i)$ $f_{12}=a_{01}+\sum_{i,j=1}^{N}a_{ij}\exp(k_i(\xi_i+\xi_j))$
VII	Homoclinic test approach[24]	$f_{11}=a_{01}+a_{11}\left(e^{ip\xi_1}+e^{-ip\xi_1}\right)e^{q\xi_2}+a_{12}e^{2q\xi_2}$
VIII	EHTA[25]	$f_{11}=a_{11}e^{\xi_1}+a_{12}\cos\xi_2+a_{13}e^{-\xi_1}$ $f_{12}=a_{11}e^{\xi_1}+a_{12}\sin\xi_2+a_{13}e^{-\xi_1}$
IX	Physics-informed neural networks method[19]	$f_{11}=a_{11}e^{\xi_1}(\cos\xi_2+a_{13}\cosh\xi_1)$ $f_{12}=a_{11}\xi_1^2+a_{12}\xi_2^2+a_{13}\cosh\xi_3$
X	Lumps and three-wave solutions[26]	$f_{11}=a_{01}+a_{11}\xi_1^2+a_{12}\xi_2^2$ $+a_{13}e^{\xi_1}+a_{13}\cos\xi_2+a_{13}e^{-\xi_1}+a_{16}\cosh\xi_3$ $f_{12}=a_{01}+a_{11}\xi_1^2+a_{12}\xi_2^2+a_{13}\cosh\xi_3$
XI	Periodic-soliton and periodic wave solutions[27]	$f_{11}=a_{11}e^{-\xi_1}+a_{12}\tan\xi_2+a_{13}\tanh\xi_3+a_{14}e^{\xi_1}$ $f_{12}=a_{11}e^{-\xi_1}+a_{12}\cos\xi_2+a_{13}\sin\xi_3+a_{14}e^{\xi_1}$ $f_{13}=a_{11}e^{-\xi_1}+a_{12}\cos\xi_2+a_{13}\sin\xi_3+a_{14}\tanh\xi_4+a_{15}e^{\xi_1}$ $f_{14}=a_{11}e^{-\xi_1}+a_{12}\cos\xi_2+a_{13}\sin\xi_3+a_{14}\cosh\xi_4+a_{15}e^{\xi_1}$
XII	Periodic wave solutions[28]	$f_{11}=a_{11}e^{-\xi_1}+a_{12}\cos\xi_2+a_{13}\tan\xi_3+a_{14}\tanh\xi_4$
XIII	Lump-soliton solutions[29]	$f_{11}=a_0+\xi_1^2+\xi_2^2+a_{11}e^{\xi_3}$ $f_{12}=a_0+\xi_1^2+\xi_2^2+a_{11}e^{\xi_3}+a_{12}e^{\xi_4}$ $f_{13}=a_0+\xi_1^2+\xi_2^2+a_{11}\cosh e^{\xi_3}$ $f_{14}=a_0+\xi_1^2+\xi_2^2+a_{11}\cosh e^{\xi_3}+a_{11}\cos e^{\xi_3}$
XIV	k-lump and k-kink solutions[30]	$f_{11}=\xi_1^4+\xi_1^2+\xi_2^2+a_{11}e^{\xi_1}$ $f_{12}=\xi_1^4+\xi_1^2+\xi_2^2+a_{11}e^{\xi_1}+a_{12}e^{\xi_2}$ $f_{13}=\xi_1^4+\xi_1^2+\xi_2^2+a_{11}\cosh\xi_2$. $f_{14}=\xi_1^4+\xi_1^2+\xi_2^2+a_{11}\cos\xi_1+a_{12}\cos\xi_2$ $f_{15}=a_0+a_{11}e^{\xi_1}\cos(\xi_1)+a_{12}e^{2\xi_1}$.

Source: created by the authors.

Figures 2–5 present kink-type waves, which represent sharp wavefronts. Physically, these describe transition layers or shock-like structures that appear in fluids or plasmas. The stability of kinks indicates persistent traveling fronts that preserve their shape. These solutions mimic internal wave boundaries or phase fronts in layered media. Figures 6–9 show rogue or localized high-amplitude waves. These waves emerge suddenly and are characterised by large peaks followed by decay. In real-world physics, rogue waves appear in deep ocean dynamics, nonlinear optics, or energy bursts in plasmas. Such patterns model instabilities or energy-focusing phenomena. Figures 10–11 (lump) and other soliton forms describe localized, smooth wave packets. These remain stable over long periods/distances without dispersion. They can travel through each other and re-emerge, a hallmark of integrable systems. Such soliton-like behaviors indicate potential applicability in optical fibre communication or quantum fluids. Figures 14–15 (peakon) and Figures 16–17 (trigonometric-hyperbolic mix) show non-smooth crested waves and periodic wave structures. Peakons have a cusp at the peak—used to model breaking waves or edges. Mixed-type solutions (trigonometric and hyperbolic) imply periodic oscillations within a solitary wave, suitable for modulated wave trains. These represent multi-scale interactions or wave interference in shallow water or stratified layers.

5. Limitation and discussion

The application of BNNM to the extended sixth-order Benney–Luke equation presents significant improvements over traditional solution techniques and prior studies focusing on standard or fractional Benney—Luke forms.[31] By incorporating higher-order nonlinear terms and dispersive effects such as u_{xxxxxx}, u_x, u_{xx}, and combinations of spatial-temporal derivatives which capture a wider range of physically relevant wave phenomena, including rogue wave formation, modulational instability, and wave interactions across different scales. Moreover, while previous efforts using methods like the tanh–coth approach, (G'/G)-expansion, or the simple Hirota method were constrained to specific types of solitary waves, the current BNNM framework enables the construction of both localized and periodic structures, including kink–antikink pairs, peakons,

Table 2. Solutions obtained from the bilinear neural network method

$u_{51} = \frac{2\begin{pmatrix} a_{51}\left(5c_{51}e^{5c_{51}(x+kt+hy)+b_{52}} + c_{51}e^{c_{51}(x+kt+hy)+c_{52}}\right)e^{-c_{51}(x+kt+hy)-c_{52}} \\ -a_{51}\left(e^{5c_{51}(x+kt+hy)+b_{52}} + e^{c_{51}(x+kt+hy)+b_{52}}\right)c_{51}e^{-c_{51}(x+kt+hy)-c_{52}} + 2a_{52}e^{2c_{51}(x+kt+hy)+2b_{52}} \end{pmatrix}}{a_{05} + a_{51}\left(e^{5c_{51}(x+kt+hy)+b_{52}} + e^{c_{51}(x+kt+hy)+c_{52}}\right)e^{-c_{51}(x+kt+hy)-c_{52}} + a_{52}e^{2c_{51}(x+kt+hy)+2c_{52}}}$
$u_{61}^1 = \frac{2a_{61}b_{61}e^{b_{61}(x+kt+hy)+b_{62}} - 2a_{62}c_{61}\sin\left(c_{61}\left(x+kt+hy\right)+c_{62}\right) - 2a_{63}b_{61}e^{-b_{61}(x+kt+hy)-b_{62}}}{a_{61}e^{b_{61}(x+kt+hy)+b_{62}} + a_{62}\cos(c_{61}(x+kt+hy)+c_{62}) + a_{63}e^{-b_{61}(x+kt+hy)-b_{62}}}$
$u_{61}^2 = \frac{2a_{61}b_{61}e^{b_{61}(x+kt+hy)+b_{62}} + 2a_{62}c_{61}\cos\left(c_{61}\left(x+kt+hy\right)+c_{62}\right) - 2a_{63}b_{61}e^{-b_{61}(x+kt+hy)-b_{62}}}{a_{61}e^{b_{61}(x+kt+hy)+b_{62}} + a_{62}\sin(c_{61}(x+kt+hy)+c_{62}) + a_{63}e^{-b_{61}(x+kt+hy)-b_{62}}}$
$u_{71} = \frac{2\left(\frac{a_{73}(2b_{71}+c_{71})(b_{71}+c_{71})^2a_{07}(b_{71}+2c_{71})b_{71}e^{\xi_1}}{(b_{71}-c_{71})^2a_{72}(2b_{71}-c_{71})(b_{71}-2c_{71})} + a_{72}c_{71}e^{\xi_2} + a_{73}(b_{71}+c_{71})e^{\xi_1+\xi_2}\right)}{\left(a_{07} + \frac{a_{73}(2b_{71}+c_{71})(b_{71}+c_{71})^2a_{07}(b_{71}+2c_{71})e^{\xi_1}}{(b_{71}-c_{71})^2a_{72}(2b_{71}-c_{71})(b_{71}-2c_{71})} + a_{72}e^{\xi_2} + a_{73}e^{(\xi_1+\xi_2}\right)}$
$u_{81} = \frac{2(a_{81}b_{81}exp(\xi_1)(\cos(\xi_2)+a_{83}\cosh(\xi_1)) + a_{81}e^{\xi_1}(-c_{81}\sin(\xi_2)+a_{83}b_{81}\sinh(\xi_1)))}{a_{81}e^{\xi_1}(\cos(\xi_2)+a_{83}\cosh(\xi_1))}$
$u_{82} = \frac{2(a_{81}b_{81}exp(\xi_1(\sin(\xi_2)+a_{83}\cosh(\xi_1) + a_{81}e^{\xi_1}(c_{81}\cos(\xi_2)+a_{83}b_{81}\sinh(\xi_1))}{a_{81}e^{\xi_1}(\sin(\xi_2)+a_{83}\cosh(\xi_1)}$

lumps, and even multi-soliton resonances. This versatility arises from the BNNM's ability to encode trial functions, weights, and activation patterns systematically using neural architectures. The resulting solutions are expressed using softmax functions, which play an important role in machine learning.[32,33] A key feature of the sixth-order extension is its ability to model wave energy transfer and dispersion more accurately, especially in high-tension surface dynamics and fluid mechanics scenarios. Furthermore, the solutions presented were tested for structural consistency with the governing bilinear form and verified through symbolic computation, strengthening their theoretical and physical relevance.

6. Conclusion

In this study, we successfully derived a rich set of analytical solutions to the extended sixth-order equation using the BNNM. The sixth-order extension marks a meaningful advancement, as it introduces complex nonlinear and dispersive terms that enable more faithful modeling of real-world wave phenomena. The neural network-based bilinear formulation not only generalises existing solution methods but also simplifies the search for diverse solution types ranging from simple kinks to highly localized rogue waves and structured soliton interactions. These findings confirm that the extended sixth-order form is not merely a mathematical curiosity but a powerful model capable of capturing intricate dynamics in nonlinear physics. Moreover, the BNNM framework offers a computationally viable and flexible approach for exploring further extensions of other nonlinear evolution equations, thus opening new research directions in mathematical physics, fluid dynamics, and soft computing.

Acknowledgments

The authors sincerely appreciate the Posts and Telecommunications Institute of Technology in Ho Chi Minh City, Vietnam for the provision of necessary resources and a conducive research environment, which contributed significantly to the success of this study.

Funding

This research accepted ID 22-2025-HV-CNTT2 with sanction number 282/QĐ-HV on 11-4-2025 from President of the Posts and Telecommunications Institute of Technology, Viet Nam.

Conflict of interest

The authors declare no conflict of interest

Author contributions

Conceptualization: Nguyen Minh Tuan
Data curation: Nguyen Minh Tuan
Investigation: Nguyen Minh Tuan
Methodology: Nguyen Minh Tuan
Software: Nguyen Minh Tuan
Validation: Huynh Trong Thua
Writing–original draft: All authors
Writing–review & editing: All authors

Availability of data

The data generated in this study are available within the manuscript.

AI tools statement

All authors confirm that no AI tools were used in the preparation of this manuscript.

References

1. Younas U, Ismael HF, Sulaiman TA, Murad MAS, Shah NA, Sharifpur M. A diversity of patterns to new (3 + 1)-dimensional Hirota bilinear equation that models dynamics of waves in fluids. *Results Phys.* 2023;54:107124. https://www.doi.org/10.1016/j.rinp.2023.107124
2. Akter J, Ali Akbar M. Exact solutions to the Benney–Luke equation and the Phi-4 equations by using modified simple equation method. *Results Phys.* 2015;5:125–130. https://www.doi.org/10.1016/j.rinp.2015.01.008
3. Ali KK, Nuruddeen R. Analytical treatment for the conformable space-time fractional Benney-Luke equation via two reliable methods. *Int J Phys Res.* 2017;5(2):109. https://www.doi.org/10.14419/ijpr.v5i2.8403
4. Durur H, Yokuş A. Exact solutions of the Benney–Luke equation via (1/G')-expansion method. *Bilecik Şeyh Edebali Üniv Fen Bilimleri Derg.* 2021;8(1):56–64. https://www.doi.org/10.35193/bseufbd.833244
5. Ersoy Hepson O. Hyperbolic tangent ansatz method to space time fractional modified KdV, modified EW and Benney-Luke Equations. *Math Comput Sci.* 2018. https://www.doi.org/10.20944/preprints201802.0141.v1
6. Ghanbari B, Inc M, Yusuf A, Baleanu D. New solitary wave solutions and stability analysis of the Benney-Luke and the Phi-4 equations in mathematical physics. *AIMS Math.* 2019;4(6):1523–1539. https://www.doi.org/10.3934/math.2019.6.1523
7. Gozukızıl ÖF, Akcagıl Ş. Travelling wave solutions to the Benney-Luke and the higher-order improved boussinesq equations of sobolev type. *Abstract Appl Anal.* 2012;2012:1–10. https://www.doi.org/10.1155/2012/890574
8. Gundogdu H, Gozukizil ÖF. On the new type of solutions to Benney-Luke equation. *Bol Soc Paranaense Mat.* 2021;39(5):103–111. https://www.doi.org/10.5269/bspm.41244
9. Hossain AKMKS, Akbar MA. Traveling wave solutions of Benny Luke equation via the enhanced (G'/G)-expansion method. *Ain Shams Eng J.* 2021;12(4):4181–4187. https://www.doi.org/10.1016/j.asej.2017.03.018
10. Islam SMR, Khan K, Woadud KMAA. Analytical studies on the Benney–Luke equation in mathematical physics. *Waves Random Complex Media.* 2018;28(2):300–309. https://www.doi.org/10.1080/17455030.2017.1342880
11. Tuan NM, Kooprasert S, Sirisubtawee S, Meesad P. The bilinear neural network method for solving Benney–Luke equation. *Partial Differ Equ Appl Math.* 2024;10:100682. https://www.doi.org/10.1016/j.padiff.2024.100682
12. Khan U, Ellahi R, Khan R, Mohyud-Din ST. Extracting new solitary wave solutions of Benny–Luke equation and Phi-4 equation of fractional order by using (G'/G)-expansion method. *Opt Quant Electron.* 2017;49(11):362. https://www.doi.org/10.1007/s11082-017-1191-4
13. Mbusi SO, Muatjetjeja B, Adem AR. Lagrangian formulation, conservation laws, travelling wave solutions: a generalized Benney-Luke equation. *Math.* 2021;9(13):1480. https://www.doi.org/10.3390/math9131480
14. DiPietro R, Hager GD. Deep learning: RNNs and LSTM. In: Handbook of medical image computing and computer assisted intervention. Elsevier; 2020:503–519. https://www.doi.org/10.1016/B978-0-12-816176-0.00026-0
15. Hirota R. Direct methods in soliton theory. In: Bullough RK, Caudrey PJ, eds. Solitons. Vol 17. Springer Berlin Heidelberg; 1980:157–176. https://www.doi.org/doi:10.1007/978-3-642-81448-8_5
16. Capetillo P, Hornewall J. Introduction to the Hirota Direct Method. 2021.
17. Liu JG, Zhu WH, Wu YK, Jin GH. Application of multivariate bilinear neural network method to fractional partial differential equations. *Results Phys.* 2023;47:106341. https://www.doi.org/10.1016/j.rinp.2023.106341
18. Lin S, Chen Y. A two-stage physics-informed neural network method based on conserved quantities and applications in localized wave solutions. *J Comput Phys.* 2022;457:111053. https://www.doi.org/10.1016/j.jcp.2022.111053

19. Miao Z, Chen Y. Physics-informed neural networks method in high-dimensional integrable systems. *Mod Phys Lett B.* 2022;36(01):2150531. https://www.doi.org/10.1142/S021798492150531X
20. Zhang RF, Bilige S. Bilinear neural network method to obtain the exact analytical solutions of nonlinear partial differential equations and its application to p-gBKP equation. *Nonlinear Dyn.* 2019;95(4):3041–3048. https://www.doi.org/10.1007/s11071-018-04739-x
21. Zhang RF, Li MC. Bilinear residual network method for solving the exactly explicit solutions of nonlinear evolution equations. *Nonlinear Dyn.* 2022;108(1):521–531. https://www.doi.org/10.1007/s11071-022-07207-x
22. Tuan NM, Meesad P. New solutions of sixth-order Benney–Luke equation using bilinear neural network method. *Z Angew Math Phys.* 2025;76(4):133. https://www.doi.org/10.1007/s00033-025-02516-8
23. Wazwaz AM. Partial differential equations and solitary waves theory. Higher Education Press; Springer; 2009.
24. Dai Z, Liu J, Li D. Applications of HTA and EHTA to YTSF Equation. *Appl Math Comput.* 2009;207(2):360–364. https://www.doi.org/10.1016/j.amc.2008.10.042
25. Zhao Z, Dai Z, Han S. The EHTA for nonlinear evolution equations. *Appl Math Comput.* 2010;217(8):4306–4310. https://www.doi.org/10.1016/j.amc.2010.09.069
26. Wang X, Bilige S. Novel interaction phenomena of the (3+1)-dimensional Jimbo–Miwa equation. *Commun Theor Phys.* 2020;72(4):045001. https://www.doi.org/10.1088/1572-9494/ab690c
27. Shen JL, Wu XY. Periodic-soliton and periodic-type solutions of the (3+1)-dimensional Boiti–Leon–Manna–Pempinelli equation by using BNNM. *Nonlinear Dyn.* 2021;106(1):831–840. https://www.doi.org/10.1007/s11071-021-06848-8
28. Feng Y, Bilige S. Various rational solutions and rogue wave solutions of extended (2+1)-dimensional Calogero-Bogoyavlenskii-Schiff-like equation. *Preprints.* 2020. https://www.doi.org/10.22541/au.160407386.60382756/v1
29. Hong B, Wang J. Exact Solutions for the Generalized Atangana-Baleanu-Riemann Fractional (3 + 1)-Dimensional Kadomtsev–Petviashvili Equation. *Symmetry.* 2022;15(1):3. https://www.doi.org/10.3390/sym15010003
30. Gu Y, Malmir S, Manafian J, et al. Variety interaction between k-lump and k-kink solutions for the (3+1)-D Burger system by bilinear analysis. *Results Phys.* 2022;43:106032. https://www.doi.org/10.1016/j.rinp.2022.106032
31. Tuan NM, Phayung M. A novel softmax method for solving second Benney-Luke equation. *J Comput Appl Math.* 2025;472:116791. https://www.doi.org/10.1016/j.cam.2025.116791
32. Tuan NM, Meesad P, Nguyen HHC. English–Vietnamese Machine Translation Using Deep Learning for Chatbot Applications. *SN Comput Sci.* 2024;5(1):5. https://www.doi.org/10.1007/s42979-023-02339-2
33. Tuan NM, Son NH. A New Softmax Method Performance for Solving Chaffee-Infante Equation. *Int J Math Comput Sci.* 2025;20(3):743–749. https://www.doi.org/10.69793/ijmcs/03.2025/tuan

Nguyen Minh Tuan *is a computer scientist from Ho Chi Minh City, Vietnam, currently affiliated with the Posts and Telecommunications Institute of Technology (PTIT). He earned his Ph.D. in Applied Mathematics and Computer Science from King Mongkut's University of Technology North Bangkok (KMUTNB), Thailand. He also holds a Master's degree in Mathematics from the University of Science, Ho Chi Minh City, and a Bachelor's degree in Mathematics and Computer Science from Can Tho University, Vietnam. From 2012 to 2020, he served as a lecturer at Ho Chi Minh City University of Technology College, where he was actively involved in teaching and research. His research interests include artificial intelligence, numerical computation, optimization algorithms, and applied mathematics in computer science. Dr. Nguyen is currently pursuing further studies at FernUniversität in Hagen, Germany, to advance his research and expertise in computer science.*
https://orcid.org/0000-0002-4035-1759

Huynh Trong Thua *is the Head of the Information Security Department, Faculty of Information Technology 2, at the Posts and Telecommunications Institute of Technology (PTIT), Vietnam. He earned his Bachelor's degree in Information Technology from Ho Chi Minh City University of Natural Sciences, his Master's degree in Computer Engineering from Kyung Hee University, Korea, and his Ph.D. in Computer Science from Ho Chi Minh City University of Technology, Vietnam National University. His research interests include cybersecurity, artificial intelligence, big data, and intelligent information systems. Dr. Huynh has published extensively in these areas and has made significant contributions to both academic and applied research communities.*
https://orcid.org/0000-0003-3934-1067

An International Journal of Optimization and Control: Theories & Applications
(https://accscience.com/journal/ijocta)